

FINEL 302

# A finite element–difference computational model for stress analysis of layered composite cylindrical shells

T. Kant and M.P. Menon

*Department of Civil Engineering, Indian Institute of Technology, Powai, Bombay-400 076, India*

Received March 1992

Revised February 1993

**Abstract.** A  $C^0$  finite element space discretization procedure is employed in a general fibre-reinforced composite cylindrical shell theory based on a higher-order displacement model. The displacement model incorporates non-linear variation of tangential displacement components through the thickness of the shell. The use of a shear correction coefficient thus becomes redundant. The discrete element chosen is a nine-noded Lagrangian quadrilateral with seven degrees of freedom per node.

Two formulations, one in which  $(h/R) \ll 1$  and another in which  $(h/R)^2 \ll 1$ , are derived. After the nodal displacements are obtained from the global finite element analysis, the secondary quantities are determined element-wise. The planar lamina stresses are computed through the constitutive relations while the transverse shear stresses are estimated by making use of the equilibrium equations. A special finite difference scheme is developed to integrate the equilibrium equations with a view to estimate transverse/interlaminar stresses across the shell thickness. The transverse/interlaminar stresses computed by the above technique do maintain the continuity at the interface of two layers. The results obtained are compared with available elasticity, closed-form and other finite element solutions.

## Introduction

Fibre-reinforced composite shells of revolution find applications in diverse branches of technology because of their high strength-to-weight and stiffness-to-weight ratios. The increased use of composites for high-performance design in aerospace applications has necessitated the need for a realistic prediction of the behaviour of these composite material structures. Experience has shown that accurate prediction of only the in-plane lamina stresses is just not adequate; the transverse and interlaminar stresses play an important role in initiating the separation of individual laminae thereby causing delamination. This results in structural and functional failure due to the destruction of the load transferring mechanism. It is thus essential to develop a theory and an associated computing algorithm which has the capability of predicting both the planar as well as the transverse stresses accurately.

A three-dimensional elasticity solution of laminated shells is extremely complex. Further more such a solution lacks generality. To simplify the governing equation system, the three-dimensional equation system is generally reduced to a two-dimensional one by incorporating certain assumptions regarding the kinematics of deformation in the thickness direction of the shell. In the classical shell theory based on the Love–Kirchhoff hypothesis [1,2], it is assumed that transverse normals remain straight and normal to the mid-surface and undergo no change in their length during deformation. The transverse strains, thus, become negligibly

*Correspondence to:* Professor Tarun Kant, Department of Civil Engineering, Indian Institute of Technology, Powai, Bombay-400 076, India.

small. The lamina is, further, assumed to be in a state of plane stress in the constitutive relation. Naghdi [3] has presented a survey of developments until 1956. Dong, Pister and Taylor [4] have extended Donnell's shallow shell theory for laminated anisotropic shells. A closed-form solution for an arbitrary laminated anisotropic cylindrical shell based on classical lamination theory is given by Chaudhuri et al. [5]. Reuter [6] has obtained closed-form solutions for balanced unsymmetric and unbalanced symmetric angle-ply cylindrical shells. The above works are based on Love's classical shell theory. The classical theory does not include the effects of transverse shear strains, transverse normal strain and transverse normal stress. A composite laminated shell should necessarily include all or at least some of these effects.

Dong and Tso [7] are the first to incorporate the effects of transverse shear deformation through the shell thickness and developed a theory for analyzing a laminated orthotropic shell. However, only problems of cylindrical shells in which the orthotropic material axes of each layer coincided with the reference axes of shell could be solved.

A number of formulations, based on the Reissner–Mindlin hypothesis of constant shear angle through the shell thickness, are presented in [8–10]. These are known as the first-order shear deformation theories. Seide and Chaudhuri [11] have presented a formulation which allows for a layer-wise (piecewise) linear approximation of the non-linear cross-sectional deformations. In a constant shear angle theory or a layer-wise constant shear angle theory, the shear correction coefficient used is problem dependent and its accurate prediction is very cumbersome. The effects of true cross-sectional warping, which is essential in laminated and sandwich shells, due to combined effects of thicknesses, lamination and anisotropy, are not taken into account in these formulations.

A further refinement of the mathematical model using assumed through-thickness displacement variations which result in a parabolic distribution of the transverse shear strains becomes essential in order to estimate lamina stresses and interlaminar transverse stresses through the thickness accurately. Higher-order shear deformation theories are formulated by expanding the continuum displacement components in the form of a power series in the transverse coordinate. Depending on the number of terms retained in the series expressions, various higher-order shell theories [12–18] have been developed.

Here, based on a higher-order displacement field a fibre-reinforced composite cylindrical shell theory, suitable for  $C^0$  finite element formulation, is developed. The interlaminar and transverse stresses are evaluated by integrating the equilibrium equations using suitable finite difference operators through the thickness. The continuity of transverse stresses at the interface of layers is maintained in this computational algorithm.

## Theoretical formulation

The displacement components  $u_i^z(\theta, x, z)$ ,  $i = 1, 2, 3$ , at any point in the shell, are expressed in the form of a power series, in powers of the thickness coordinate  $z$ . The coordinate system is shown in Fig. 1. The displacement component  $u_3^z$  is assumed to be constant through the shell thickness. The theory is based on the displacement model,

$$\begin{aligned} u_i^z &= u_i + z\alpha_i + z^3\alpha_i^* \quad (i = 1, 2), \\ u_3^z &= u_3, \end{aligned} \quad (1)$$

in which  $u_1$ ,  $u_2$  and  $u_3$  are the displacements of a point in the  $\theta$ ,  $x$ - and  $z$ -direction respectively and  $\alpha_1$  and  $\alpha_2$  are the rotations of the  $\theta$ -axis and  $x$ -axis respectively. The other terms,  $\alpha_1^*$  and  $\alpha_2^*$ , correspond to higher-order terms in the Taylor's series expansion. These

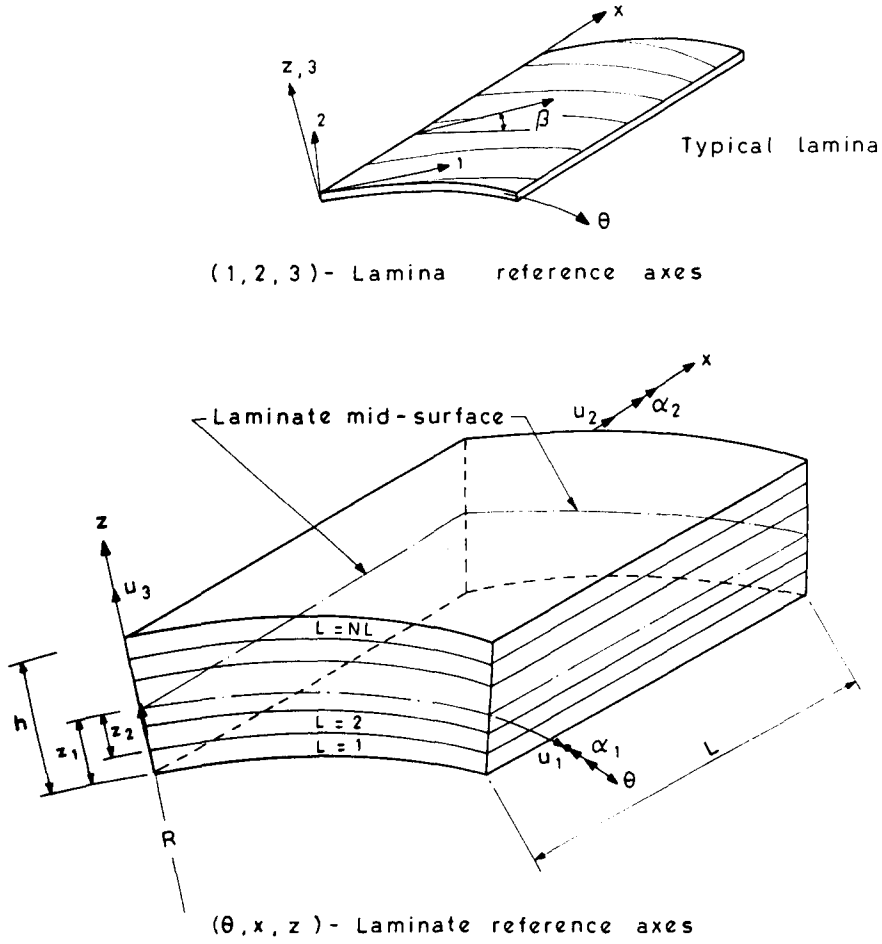


Fig. 1. Laminate geometry and positive set of lamina/laminate reference axes, displacement components and fibre orientations.

displacements are defined at the mid-surface reference plane. Thus the generalized displacement vector  $d$  of the reference plane is defined as:

$$d = (u_1, u_2, u_3, \alpha_1, \alpha_2, \alpha_1^*, \alpha_2^*)^t. \quad (2)$$

By substituting eqn. (1) into the strain-displacement relations of the classical theory of elasticity particularized for a cylindrical shell [2,14], the following relationships are obtained.

• *Theory 1* (wherein terms of order  $(h/R)$  and higher are assumed small compared to unity):

$$\begin{aligned} \epsilon_{\theta}^z &= (\epsilon_{\theta}^0 + z\chi_{\theta}^0 + z^3\chi_{\theta}^*), \\ \epsilon_x^z &= (\epsilon_x^0 + z\chi_x^0 + z^3\chi_x^*), \\ \gamma_{\theta x}^z &= (\epsilon_{\theta x}^0 + z\chi_{\theta x}^0 + z^3\chi_{\theta x}^*), \\ \gamma_{xz}^z &= (\phi_x + z^2\phi_x^*), \\ \gamma_{\theta z}^z &= (\phi_{\theta} + z^2\phi_{\theta}^*), \end{aligned} \quad (3a)$$

where  $\epsilon_{\theta}$ ,  $\epsilon_x$ ,  $\epsilon_{\theta x}$  etc. are the mid-surface strains and are defined in [18].

• *Theory 2* (wherein terms of order  $(h/R)^2$  and higher are assumed small compared to unity):

$$\begin{aligned}\epsilon_{\theta}^z &= (\epsilon_{\theta}^0 + z\chi_{\theta}^0 + z^3\chi_{\theta}^{*})/(1 + z/R), \\ \epsilon_x^z &= (\epsilon_x^0 + z\chi_x^0 + z^3\chi_x^{*}), \\ \gamma_{\theta x}^z &= (\epsilon_{\theta x}^0 + z\chi_{\theta x}^0 + z^3\chi_{\theta x}^{*})/(1 + z/R) + (\epsilon_{x\theta}^0 + z\chi_{x\theta}^0 + z^3\chi_{x\theta}^{*}), \\ \gamma_{xz}^z &= (\phi_x + z^2\phi_x^{*}), \\ \gamma_{\theta z}^z &= (\phi_{\theta} + z^2\phi_{\theta}^{*} + z^3\psi_{\theta}^{*})/(1 + z/R),\end{aligned}\quad (3b)$$

where  $\phi_{\theta}^{*} = 3\alpha_1^{*}$  and all other terms are defined in [18].

The generalized strain vector  $\bar{\epsilon}$  defining strain quantities on the middle surface may be written as:

$$\bar{\epsilon} = [\epsilon_{\theta}^0, \epsilon_x^0, \epsilon_{\theta x}^0, \chi_{\theta}^0, \chi_x^0, \chi_{\theta x}^0, \chi_{\theta}^{*}, \chi_x^{*}, \chi_{\theta x}^{*}, \phi_x^0, \phi_{\theta}^0, \phi_x^{*}, \phi_{\theta}^{*}]^t \quad (4a)$$

and

$$\bar{\epsilon} = [\epsilon_{\theta}^0, \epsilon_x^0, \epsilon_{\theta x}^0, \epsilon_{x\theta}^0, \chi_{\theta}^0, \chi_{\theta x}^0, \chi_{x\theta}^0, \phi_{\theta}^{*}, \chi_x^{*}, \chi_{\theta x}^{*}, \phi_{x\theta}^{*}, \phi_x^0, \phi_{\theta}^0, \phi_x^{*}, \phi_{\theta}^{*}, \psi_{\theta}^{*}]^t, \quad (4b)$$

corresponding to Theory 1 (eqn. 3a) and Theory 2 (eqn. 3b) respectively.

The stress-strain relationship for the  $L$ th lamina of the composite laminate with reference to fibre-axes (1, 2, 3) (see Fig. 1) in a compacted form is as follows:

$$\sigma_i' = C_{ij}^L \epsilon_j', \quad (5a)$$

in which,

$$\begin{aligned}\sigma' &= [\sigma_1, \sigma_2, \tau_{12}, \tau_{23}, \tau_{13}]_L^t, \\ \epsilon' &= [\epsilon_1, \epsilon_2, \gamma_{12}, \gamma_{23}, \gamma_{13}]_L^t,\end{aligned}\quad (5b)$$

and  $C_{ij}^L$  is the standard material stiffness matrix [19] with respect to the principal material directions of the  $L$ th lamina. These vectors ( $\sigma'$  and  $\epsilon'$ ) are transformed to shell coordinates  $(\theta, x, z)$  using the transformation rule of stresses and tensorial strains [20]. The stress-strain relation in the shell coordinates is written as

$$\sigma = Q^L \epsilon, \quad (6a)$$

in which

$$\begin{aligned}\sigma &= [\sigma_{\theta}, \sigma_x, \tau_{\theta x}, \tau_{xz}, \tau_{\theta z}]_L^t, \\ \epsilon &= [\epsilon_{\theta}, \epsilon_x, \gamma_{\theta x}, \gamma_{xz}, \gamma_{\theta z}]_L^t, \\ Q^L &= T^{-1} C^L (T^{-1})^t,\end{aligned}\quad (6b)$$

for the  $L$ th lamina.  $T$  is the transformation matrix and superscripts  $t$  and  $-1$  represent the transpose and the inverse of an array/square matrix, respectively.

The total potential energy  $\Pi$  for the present theory is given by

$$\Pi = \frac{1}{2} \int_V \epsilon^t \sigma \, dV - \int_A d^t q \, dA, \quad (7a)$$

where  $\mathbf{q}$  represents the equivalent load vector corresponding to the seven degrees of freedom at a point on the middle surface defined by  $\mathbf{d}^t$ . The above expression can be rewritten as,

$$\Pi = \frac{1}{2} \int_A \left( \int \boldsymbol{\epsilon}^t \boldsymbol{\sigma} dz \right) dA - \int_A \mathbf{d}^t \mathbf{q} dA. \quad (7b)$$

By substituting the strain components given by eqn. (3) in eqn. (7b) and carrying out explicit integration through the shell thickness, one obtains,

$$\Pi = \frac{1}{2} \int_A \bar{\boldsymbol{\epsilon}}^t \bar{\boldsymbol{\sigma}} dA - \int_A \mathbf{d}^t \mathbf{q} dA, \quad (8)$$

in which

$$\bar{\boldsymbol{\sigma}} = [N_\theta, N_x, N_{\theta x}, M_\theta, M_x, M_{\theta x}, M_\theta^*, M_x^*, M_{\theta x}^*, Q_x, Q_\theta, Q_x^*, Q_\theta^*]^t \quad (9a)$$

and

$$\bar{\boldsymbol{\sigma}} = [N_\theta, N_x, N_{\theta x}, N_{x\theta}, M_\theta, M_x, M_{\theta x}, M_{x\theta}, M_\theta^*, M_x^*, M_{\theta x}^*, M_{x\theta}^*, Q_x, Q_\theta, Q_x^*, Q_\theta^*, S_\theta^*]^t \quad (9b)$$

are the stress-resultant vectors corresponding to the middle surface strain definitions given by eqn. (3a) and eqn. (3b) for Theory 1 and Theory 2 respectively. The relation between stress-resultant and generalized strain vectors can be concisely expressed as:

$$\bar{\boldsymbol{\sigma}} = \mathbf{D} \bar{\boldsymbol{\epsilon}} \quad (10a)$$

or

$$\begin{bmatrix} N \\ M \\ M^* \\ Q \\ Q^* \end{bmatrix} = \begin{bmatrix} D_m & D_c & \mathbf{0} \\ D_c^t & D_b & \mathbf{0} \\ \mathbf{0} & \mathbf{0} & D_s \end{bmatrix} \begin{bmatrix} \boldsymbol{\epsilon}^o \\ \boldsymbol{\kappa}^o \\ \boldsymbol{\phi}^o \end{bmatrix} \quad (10b)$$

in which the components of the stress-resultant vector and generalized strain vector are:

$$\begin{aligned} N &= (N_\theta, N_x, N_{\theta x})^t, \\ M &= (M_\theta, M_x, M_{\theta x})^t, & M^* &= (M_\theta^*, M_x^*, M_{\theta x}^*)^t, \\ Q &= (Q_x, Q_\theta)^t, & Q^* &= (Q_x^*, Q_\theta^*)^t, \\ \boldsymbol{\epsilon}^o &= (\epsilon_\theta^o, \epsilon_x^o, \epsilon_{\theta x}^o)^t, \\ \boldsymbol{\kappa}^o &= (\kappa_\theta^o, \kappa_x^o, \kappa_{\theta x}^o)^t, & \boldsymbol{\kappa}^* &= (\kappa_\theta^*, \kappa_x^*, \kappa_{\theta x}^*)^t, \\ \boldsymbol{\phi}^o &= (\phi_x, \phi_\theta)^t, & \boldsymbol{\phi}^* &= (\phi_x^*, \phi_\theta^*)^t, \end{aligned} \quad (10c)$$

corresponding to the mid-surface strain definition given by eqn. (3a) for Theory 1, and

$$\begin{aligned} N &= (N_\theta, N_x, N_{\theta x}, N_{x\theta})^t, \\ M &= (M_\theta, M_x, M_{\theta x}, M_{x\theta})^t, & M^* &= (M_\theta^*, M_x^*, M_{\theta x}^*, M_{x\theta}^*)^t \\ Q &= (Q_x, Q_\theta)^t, & Q^* &= (Q_x^*, Q_\theta^*, S_\theta^*)^t \\ \boldsymbol{\epsilon}^o &= (\epsilon_\theta^o, \epsilon_x^o, \epsilon_{\theta x}^o, \epsilon_{x\theta}^o)^t, \\ \boldsymbol{\kappa}^o &= (\kappa_\theta^o, \kappa_x^o, \kappa_{\theta x}^o, \kappa_{x\theta}^o)^t, & \boldsymbol{\kappa}^* &= (\kappa_\theta^*, \kappa_x^*, \kappa_{\theta x}^*, \kappa_{x\theta}^*)^t \\ \boldsymbol{\phi}^o &= (\phi_x, \phi_\theta)^t, & \boldsymbol{\phi}^* &= (\phi_x^*, \phi_\theta^*, \psi_\theta^*)^t \end{aligned} \quad (10d)$$

corresponding to the mid-surface strain definition given by Eq. (3b) for Theory 2. The different submatrices are defined as:

$$\begin{aligned} D_m &\text{—membrane,} & D_c &\text{—membrane–flexure coupling,} \\ D_b &\text{—flexure,} & D_s &\text{—shear.} \end{aligned}$$

The interlaminar stresses ( $\tau_{xz}$ ,  $\tau_{\theta z}$ ) cannot be accurately estimated using eqn. (6a). This is because the interlaminar stresses evaluated by this constitutive relation lead to the discontinuity at the laminae interfaces and thus violate the equilibrium conditions. For this reason, the following equilibrium equations of elasticity for each layer are used to derive expressions for transverse shear stresses in the  $L$ th lamina of a multilayered laminated shell.

$$\begin{aligned} \frac{1}{AR} \frac{\partial \sigma_\theta}{\partial \theta} + \frac{\partial \tau_{\theta x}}{\partial x} + \frac{\partial \tau_{\theta z}}{\partial z} + \frac{2}{AR} \tau_{\theta z} &= 0, \\ \frac{1}{AR} \frac{\partial \tau_{\theta x}}{\partial \theta} + \frac{\partial \sigma_x}{\partial x} + \frac{\partial \tau_{xz}}{\partial z} + \frac{1}{AR} \tau_{xz} &= 0, \end{aligned} \quad (11a)$$

where  $A = 1$  and  $(1 + z/R)$  for Theory 1 and Theory 2 respectively. In the above equation, the body forces are neglected. The above equilibrium equations are rewritten as,

$$\begin{aligned} \frac{\partial \tau_{\theta z}}{\partial z} + \frac{2}{AR} \tau_{\theta z} &= - \left( \frac{1}{AR} \frac{\partial \sigma_\theta}{\partial \theta} + \frac{\partial \tau_{\theta x}}{\partial x} \right), \\ \frac{\partial \tau_{xz}}{\partial z} + \frac{1}{AR} \tau_{xz} &= - \left( \frac{1}{AR} \frac{\partial \tau_{\theta x}}{\partial \theta} + \frac{\partial \sigma_x}{\partial x} \right). \end{aligned} \quad (11b)$$

### Finite element discretization

The generalized displacement vector  $\mathbf{d}$  and the nodal displacement vector  $\mathbf{d}_i$  are related with the aid of shape functions as follows:

$$\mathbf{d} = \sum_{i=1}^{NN} N_i(\theta, x) \mathbf{d}_i, \quad (12)$$

where NN stands for number of nodes per element. With the help of eqns. (4) and (12), the generalized strain vector  $\bar{\boldsymbol{\epsilon}}$  at any point is expressed in discrete form as follows:

$$\bar{\boldsymbol{\epsilon}} = \sum_{i=1}^{NN} \mathbf{B}_i \mathbf{d}_i, \quad (13)$$

in which  $\mathbf{B}_i$  represents the derivatives of the shape functions. The definition of the  $\mathbf{B}$  matrix is given elsewhere [18].

Having obtained the elasticity matrix  $\mathbf{D}$  as defined in eqn. (10a) and matrix  $\mathbf{B}_i$  as defined in eqn. (13), the element stiffness matrix  $\mathbf{K}^e$  can be readily computed by using the standard relation [21],

$$\mathbf{K}_{ij}^e = \int_A \mathbf{B}_i^t \mathbf{D} \mathbf{B}_j \, dA = \int_{-1}^{+1} \int_{-1}^{+1} \mathbf{B}_i^t \mathbf{D} \mathbf{B}_j |J| \, \partial \xi \, \partial \eta. \quad (14)$$

The computation of the element stiffness matrix is economized by explicit multiplication of  $\mathbf{B}_i^t$ ,  $\mathbf{D}$  and  $\mathbf{B}_j$  matrices instead of carrying out the full matrix multiplication of the triple product and due to symmetry of the stiffness matrix, only the blocks  $\mathbf{K}_{ij}$  lying on one side of

the main diagonal are formed [22]. The formulation of a consistent element load vector  $P^e$  is given in [18]. The discrete governing equilibrium equation is

$$Ka = P, \quad (15)$$

in which  $a$  is the global vector of unknown displacements,  $K$  is the global stiffness matrix and the global nodal force vector is given by  $P$ . The global stiffness matrix and global load vector are computed in the usual manner as follows:

$$K = \sum_{e=1}^{NE} K^e, \quad P = \sum_{e=1}^{NE} P^e \quad (16)$$

The governing equation given by eqn. (15) is solved for a discrete set of unknown displacements. From these the strains within a particular element and the corresponding stresses are calculated using eqns. (4) and (6) respectively. The transverse shear stresses thus obtained by eqn. (6) are found to be discontinuous at the interface of two layers of different properties. Thus as mentioned previously, a rational approach is to evaluate the transverse/interlaminar stresses by eqn. (11b).

The first task in integrating these equilibrium equations is to obtain the derivatives of the in-plane stresses. This is proposed to be obtained here by an exact surface fitting method. In this method, the surface parallel components of the stresses ( $\sigma_\theta$ ,  $\sigma_x$ ,  $\tau_{\theta x}$ ) are evaluated through constitutive relations at different Gauss points on any surface of the shell at a distance  $z$  from the mid-surface. The variation of these stresses within the element are expressed using a polynomial in  $(\theta, x)$ -coordinates. Thus we have

$$\begin{aligned} \sigma_\theta(z) &= C_1^1 + C_2^1 R\theta + C_3^1 x + C_4^1 (R\theta)^2 + C_5^1 (R\theta)x + C_6^1 x^2 + C_7^1 (R\theta)^2 x \\ &\quad + C_8^1 (R\theta)x^2 + C_9^1 (R\theta)^2 x^2, \\ \sigma_x(z) &= C_1^2 + C_2^2 R\theta + C_3^2 x + C_4^2 (R\theta)^2 + C_5^2 (R\theta)x + C_6^2 x^2 + C_7^2 (R\theta)^2 x \\ &\quad + C_8^2 (R\theta)x^2 + C_9^2 (R\theta)^2 x^2, \\ \tau_{\theta x}(z) &= C_1^3 + C_2^3 R\theta + C_3^3 x + C_4^3 (R\theta)^2 + C_5^3 (R\theta)x + C_6^3 x^2 + C_7^3 (R\theta)^2 x \\ &\quad + C_8^3 (R\theta)x^2 + C_9^3 (R\theta)^2 x^2, \end{aligned} \quad (17)$$

where  $C_1^i$  to  $C_9^i$  ( $i = 1, 2, 3$ ) are the constants of the polynomial to be evaluated.

Here the polynomials are truncated after nine terms and hence have nine constants which are evaluated for each tangential stress by utilizing the stress values at nine known Gauss points. Having computed these constants of eqn. (17), the polynomial expressions are then differentiated with respect to  $(\theta, x)$  and the expressions for the first derivatives of the in-plane stresses are obtained. These are given as follows:

$$\begin{aligned} \frac{1}{R} \frac{\partial \sigma_\theta(z)}{\partial \theta} &= C_2^1 + 2C_4^1 R\theta + C_5^1 x + 2C_7^1 R\theta x + C_8^1 x^2 + 2C_9^1 R\theta x^2, \\ \frac{\partial \sigma_x(z)}{\partial x} &= C_3^2 + C_5^2 R\theta + 2C_6^2 x + C_7^2 (R\theta)^2 + 2C_8^2 R\theta x + 2C_9^2 (R\theta)^2 x, \\ \frac{1}{R} \frac{\partial \tau_{\theta x}(z)}{\partial \theta} &= C_2^3 + 2C_4^3 R\theta + C_5^3 x + 2C_7^3 R\theta x + C_8^3 x^2 + 2C_9^3 R\theta x^2, \\ \frac{\partial \tau_{\theta x}(z)}{\partial x} &= C_3^3 + C_5^3 R\theta + 2C_6^3 x + C_7^3 (R\theta)^2 + 2C_8^3 R\theta x + 2C_9^3 (R\theta)^2 x. \end{aligned} \quad (18)$$

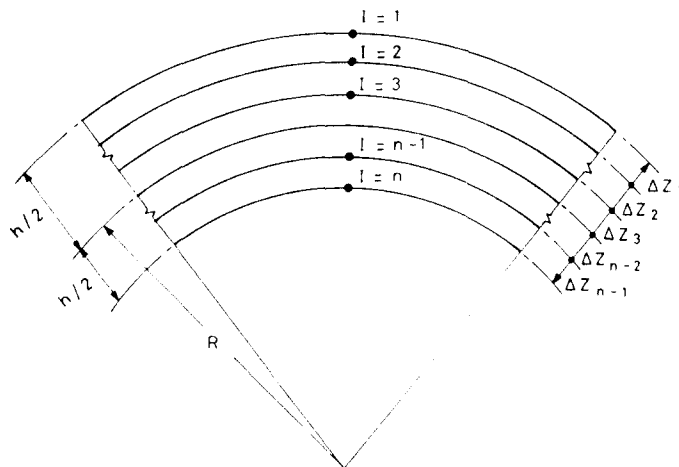


Fig. 2. Typical cross section of a shell showing unequal spacing of pivot points.

In the present study, the values of these derivatives are obtained at four Gauss points corresponding to a  $2 \times 2$  Gauss quadrature rule for shear, thus evaluating the right-hand side of eqn. (11b). These are obtained for different pivot points at known intervals in the thickness directions (see Fig. 2) at each Gauss point. The transverse shear stress variations through-the-thickness are now evaluated by integrating the equilibrium equation (11b), using a finite difference technique. Two well known finite difference schemes—(a) forward difference technique and (b) central difference technique—are used to evaluate the transverse shear stresses at different points in the thickness direction. The finite difference form of eqn. (11b) can be expressed as,

#### Forward difference technique

$$\begin{aligned} \frac{\tau_{\theta z(l+1)} - \tau_{\theta z(l)}}{\Delta z_l} + \frac{2\tau_{\theta z(l)}}{A_{(l)}R} &= - \left( \frac{1}{AR} \frac{\partial \sigma_\theta}{\partial \theta} + \frac{\partial \tau_{\theta x}}{\partial x} \right)_{(l)} \\ \Rightarrow \tau_{\theta z(l+1)} &= \Delta z_l \left( - \frac{1}{AR} \frac{\partial \sigma_\theta}{\partial \theta} - \frac{\partial \tau_{\theta x}}{\partial x} - \frac{2}{AR} \tau_{\theta z} \right)_{(l)} + \tau_{\theta z(l)}, \\ \frac{\tau_{xz(l+1)} - \tau_{xz(l)}}{\Delta z_l} + \frac{\tau_{xz(l)}}{A_{(l)}R} &= - \left( \frac{1}{AR} \frac{\partial \tau_{\theta x}}{\partial \theta} + \frac{\partial \sigma_x}{\partial x} \right)_{(l)} \\ \Rightarrow \tau_{xz(l+1)} &= \Delta z_l \left( - \frac{1}{AR} \frac{\partial \tau_{\theta x}}{\partial \theta} - \frac{\partial \sigma_x}{\partial x} - \frac{\tau_{xz}}{AR} \right)_{(l)} + \tau_{xz(l)}. \end{aligned} \quad (19a)$$

For shells with shear-free surfaces, we have  $\tau_{\theta z(1)} = 0$  and  $\tau_{xz(1)} = 0$ . With this as the starting values, the values of the transverse shear stresses are evaluated at all the other points through-the-thickness of the shell. The other shear-free surface conditions are not utilized, although they are available, because we are dealing with first-order differential equations in  $\tau_{xz}$  and  $\tau_{\theta z}$  which need only one initial condition. This is a physical paradox.

#### Central difference technique

$$\frac{\tau_{\theta z(l+1)} - (1 - Z^2)\tau_{\theta z(l)} - Z^2\tau_{\theta z(l-1)}}{Z(Z+1)\Delta z_l} + \frac{2\tau_{\theta z(l)}}{A_{(l)}R} = P_{(l)}$$

where

$$P_{(I)} = - \left( \frac{1}{AR} \frac{\partial \sigma_\theta}{\partial \theta} + \frac{\partial \tau_{\theta x}}{\partial x} \right)_{(I)},$$

$$\Rightarrow \tau_{\theta z(I+1)} = Z(Z+1)\Delta z_I \left( P - \frac{2}{AR} \tau_{\theta z} \right)_{(I)} + (1-Z^2)\tau_{\theta z(I)} + Z^2\tau_{\theta z(I-1)}; \tag{19b}$$

$$\frac{\tau_{xz(I+1)} - (1-Z^2)\tau_{xz(I)} - Z^2\tau_{xz(I-1)}}{Z(Z+1)\Delta z_I} + \frac{\tau_{xz(I)}}{A_{(I)}R} = Q_{(I)},$$

where

$$Q_{(I)} = - \left( \frac{1}{AR} \frac{\partial \tau_{\theta x}}{\partial \theta} + \frac{\partial \sigma_x}{\partial x} \right)_{(I)},$$

$$\Rightarrow \tau_{xz(I+1)} = Z(Z+1)\Delta z_I \left( Q - \frac{1}{AR} \tau_{xz} \right)_{(I)} + (1-Z^2)\tau_{xz(I)} + Z^2\tau_{xz(I-1)},$$

Here,  $Z = \Delta z_{I-1} / \Delta z_I$  [23]. Assuming that  $\tau_{xz}$  and  $\tau_{\theta z}$  at  $I=1$  are equal to zero for a shear-free surface, the values of  $\tau_{xz}$  and  $\tau_{\theta z}$  at  $I=2$  are calculated using eqn. (19a). Knowing the values now, at two points, the transverse shear stresses at all the other points through-the thickness of the shell are computed using eqn. (19b). At the interface, while setting up the equation, the values of  $P$  and  $Q$  taken are the averages of those at the top of the first layer and the bottom of the second layer.

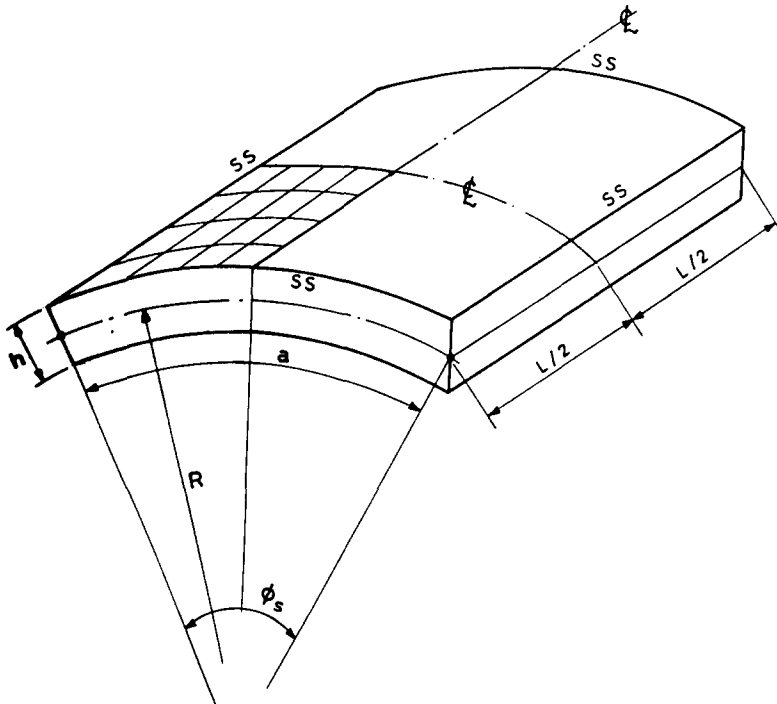


Fig. 3. Geometry and mesh pattern for a circular cylindrical roof.

### Numerical results and discussion

The proposed algorithms developed in the earlier section are tested on a few bench-mark problems. These are described below.

#### Example 1

An analysis of a layered laminated circular cylindrical shell roof with simply supported edges is carried out and the results are compared with available elasticity solution and

Table 1  
Maximum displacement and stresses for a simply supported two-layered  $90^\circ/0^\circ$  laminated cylindrical shell roof for different  $R/h$  ratios

Quantity	$R/h$	FOST		Present		Ref. [24]	
		Theory 1	Theory 2	Theory 1	Theory 2	Exact	CLT
$\bar{u}_3$	100	1.100 (1.0) <sup>a</sup>	1.108 (1.7)	1.100 (1.0)	1.108 (1.7)	1.089	1.054 (3.2)
	10	4.477 (5.3)	4.750 (11.7)	4.425 (4.1)	4.695 (10.4)	4.250	3.626 (-14.7)
	5	6.152 (6.5)	6.905 (19.6)	5.934 (2.7)	6.662 (15.3)	5.774	3.540 (-38.6)
	2	16.637 (3.5)	21.943 (35.6)	15.154 (-5.6)	19.963 (24.2)	16.062	3.092 (-80.7)
$\bar{\sigma}_\theta(z = +h/2)$	100	-0.597 (0.8)	-0.598 (1.0)	-0.597 (0.8)	-0.599 (1.0)	-0.592	-0.561 (5.2)
	10	-2.081 (-6.1)	-2.126 (-4.1)	-2.118 (-4.4)	-2.166 (-2.3)	-2.217	-2.023 (-8.7)
	5	-2.129 (-15.4)	-2.223 (-11.7)	-2.275 (-9.7)	-2.378 (-5.6)	-2.519	-2.047 (-18.7)
	2	-2.182 (-44.2)	-2.440 (-37.6)	-2.856 (-27.0)	-3.216 (-17.8)	-3.914	-1.990 (-49.1)
$\bar{\sigma}_r(z = -h/2)$	100	0.480 (-3.0)	0.484 (-2.2)	0.480 (-3.0)	0.484 (-2.2)	0.495	0.480 (-3.0)
	10	0.248 (-18.6)	0.266 (-12.7)	0.245 (-19.6)	0.263 (-13.7)	0.305	0.264 (-13.4)
	5	0.201 (-29.2)	0.231 (-18.6)	0.194 (-31.7)	0.223 (-21.5)	0.284	0.183 (-35.5)
	2	0.253 (-50.9)	0.359 (-30.4)	0.229 (-55.6)	0.325 (-37.0)	0.516	0.123 (-76.1)
$\bar{\tau}_{\theta r}(z = \pm h/2)$	100	0.034 (-2.8)	0.034 (-2.8)	0.034 (-2.8)	0.034 (-2.8)	0.035	0.033 (-5.7)
		0.050 (0.0)	0.050 (0.0)	0.050 (0.0)	0.050 (0.0)	0.050	0.049 (-2.0)
	10	-0.016 (60.0)	-0.015 (50.0)	-0.016 (60.0)	-0.015 (50.0)	-0.010	-0.011 (10.0)
		0.045 (-6.2)	0.047 (-2.0)	0.045 (-6.2)	0.047 (-2.0)	0.048	0.043 (-10.4)
	5	-0.028 (40.0)	-0.027 (35.0)	-0.028 (40.0)	-0.028 (40.0)	-0.020	-0.018 (-10.0)
		0.045 (-8.6)	0.049 (0.0)	0.044 (-10.2)	0.049 (0.0)	0.049	0.036 (-2.6)
	2	-0.034 (-5.6)	-0.035 (-2.8)	-0.035 (-2.8)	-0.037 (2.8)	-0.036	-0.020 (-44.4)
		0.064 (-14.6)	0.088 (17.3)	0.064 (-14.6)	0.089 (18.6)	0.075	0.028 (-62.7)

<sup>a</sup> Percentage difference.

Table 2  
Maximum transverse shear stress ( $\bar{\tau}_{\theta z}$ ) for a simply supported two layered  $90^\circ/0^\circ$  laminated cylindrical shell roof for different  $R/h$  ratios at ( $z = h/4$ )

$R/h$	Models	Theory 1		Theory 2	
		CD	FD	CD	FD
100	FOST	0.2424 (2.4) <sup>a</sup>	0.2323 (-1.8)	0.2424 (2.4)	0.2324 (-1.8)
	Present	0.2424 (2.4)	0.2323 (-1.8)	0.2424 (2.4)	0.2324 (-1.8)
	Exact [24]			0.2367	
10	FOST	0.8220 (-5.4)	0.7859 (-9.6)	0.8216 (-5.5)	0.7871 (-9.5)
	Present	0.8241 (-5.1)	0.7871 (-9.4)	0.8238 (-5.2)	0.7882 (-9.3)
	Exact [24]			0.8691	
5	FOST	0.9314 (2.6)	0.8936 (-1.4)	0.9302 (2.4)	0.8956 (-1.3)
	Present	0.9339 (2.8)	0.8924 (-1.6)	0.9328 (2.7)	0.8948 (-1.4)
	Exact [24]			0.9076	
2	FOST	0.8623 (-3.1)	0.8220 (-7.6)	0.8849 (-0.5)	0.8576 (-3.6)
	Present	0.8723 (-1.9)	0.8165 (-8.2)	0.9008 (1.1)	0.8523 (-4.2)
	Exact [24]			0.8900	

<sup>a</sup> Percentage difference.

classical lamination theory solution (CLT) given by Ren [24]. The shell roof has a radius  $R = 5$  in., length  $L = 30$  in. and subtended angle  $\phi_s = \pi/3$ . A sinusoidal load,  $p = p_0 \sin(\pi\theta/\phi_s) \sin(\pi x/L)$  is applied on the shell surface (see Fig. 3). Two fibre orientations,  $90^\circ/0^\circ$  and  $0^\circ/90^\circ/0^\circ$ , are considered. Their thicknesses are  $h/2$  and  $h/2$  and  $h/4$ ,  $h/2$  and  $h/4$  respectively. The lamina material properties are:

$$E_1 = 25E_2, \quad E_3 = E_2, \quad G_{12} = G_{13} = 0.5E_2, \quad G_{23} = 0.2E_2, \\ \nu_{12} = \nu_{13} = \nu_{23} = 0.25.$$

Numerical results are obtained for different  $R/h$  ratios, namely 100, 10, 5, and 2. For the  $90^\circ/0^\circ$  shell, the normalized transverse deflection and in-plane stresses are given in Table 1 and the normalized transverse shear stresses are given in Table 2. For the  $0^\circ/90^\circ/0^\circ$  shell, the normalized transverse deflection and in-plane stresses are given in Table 3 and the transverse shear stresses are plotted in Figs. 4 and 5 for  $R/h = 10$  and 5 respectively. The maximum deflections and the normal stresses at the center and transverse shear stresses at supports are normalized as follows:

$$(\bar{\sigma}_\theta, \bar{\sigma}_x) = \frac{1}{p_0 s^2} (\sigma_\theta, \sigma_x), \quad (\bar{\tau}_{\theta z}, \bar{\tau}_{xz}) = (\tau_{\theta z}, \tau_{xz}) / p_0 s, \\ \bar{u}_3 = \frac{10E_2 u_3}{p_0 h s^4}, \quad \bar{u}_1 = \frac{100E_2 u_1}{p_0 h s^4}, \quad s = R/h.$$

The percentage difference between the present and the elasticity solutions is presented in the respective tables. It is observed from these results that for lower  $R/h$  ratios, both stress and displacement fields, given by the present formulation, are close to the exact three-dimen-

Table 3  
Maximum stresses and displacement for a simply supported three-layered 0°/90°/0° laminated cylindrical shell roof for different R/h ratios

R/h	Theory	$\bar{u}_3$	$\bar{\sigma}_\theta$ (z = ± h/2)	$\bar{\sigma}_x$ (z = ± h/2)	$\tau_{\theta x}$ (z = ± h/2)	$\bar{\tau}_{zx}(z = -h/4)$		$\bar{\tau}_{\theta z}(z = -h/4)$	
						FD	CD	FD	CD
100	Present Theory 1	0.542	0.539	0.0153	-0.0168	0.0163	0.0168	0.299	0.293
		(-1.9)	(-2.5) <sup>a</sup>	(-2.5)	(-3.5)	(-7.3)	(-4.5)	(-3.5)	(-5.5)
		-0.533	-0.0031	0.0247					
		(-2.7)	(-3.1)	(-2.3)					
Present Theory 2	0.545	0.541	0.0153	0.0170	0.0163	0.0169	0.299	0.289	
	(-1.4)	(-2.1)	(-2.5)	(-2.2)	(-7.3)	(-3.9)	(-3.5)	(-6.7)	
		-0.537	-0.0031	0.0247					
		(-2.0)	(-3.1)	(-2.3)					
Exact solution [24]	0.553	0.553	0.0157	-0.0174	0.0176		0.310		
		-0.548	-0.0032	0.0253					
CLT [26]	0.538	0.543	0.0153	-0.0168	-		-		
	(-2.7)	(-1.8)	(-2.5)	(-3.4)					
		-0.537	-0.0030	-0.0248					
		(-2.0)	(-6.2)	(-1.9)					
10	Present Theory 1	1.450	0.915	0.0136	-0.0032	0.0093	0.0091	0.455	0.438
		(-8.0)	(-4.4)	(-20.0)	(3.22)	(-12.2)	(-14.1)	(-10.8)	(-14.1)
		0.997	-0.0094	0.0145					
		(-5.7)	(-5.0)	(-5.2)					
Present Theory 2	1.522	0.940	0.0140	-0.0028	0.0095	0.0093	0.459	0.443	
	(-3.5)	(-1.8)	(-17.0)	(-9.7)	(-10.4)	(-12.2)	(-10.0)	(-13.1)	
		-1.077	-0.0102	0.0151					
		(1.79)	(3.03)	(-1.3)					
Exact solution [24]	1.577	0.957	0.0170	-0.0031	0.0106		0.510		
		-1.058	-0.0099	0.0153					
CLT [26]	0.843	0.821	0.0108	-0.0030	-		-		
	(-46.5)	(-14)	(-36)	(-3.2)					
		-0.869	-0.0084	0.0095					
		(-17)	(-15)	(-37.9)					
5	Present Theory 1	3.226	1.190	0.0190	-0.0102		0.0116	0.380	
		(-12.7)	(-4.9)	(-38.0)	(6.25)	(-30.5)	(-28.7)		
		-1.323	-0.0146	0.0226					
		(-15.0)	(-14.0)	(-11.7)					
Present Theory 2	3.540	1.240	0.0200	-0.0092		0.0121	0.388		
	(-4.2)	(-0.9)	(-34.0)	(-4.2)	(-27.5)	(-27.2)			
		-1.561	-0.0171	0.0251					
		(-0.1)	(-0.6)	(-1.9)					
Exact solution [24]	3.694	1.252	0.0306	-0.0096		0.0167	0.533		
		-1.562	-0.0170	0.0256					
2	Present Theory 1	13.852	2.307	0.0426	-0.0389		0.0361	0.212	
		(-17.2)	(-12.0)	(-62.0)	(11.1)	(-21.0)	(-61.5)		
		-2.610	-0.0356	0.0605					
		(-33.0)	(-27.0)	(-19.0)					
Present Theory 2	17.062	2.415	0.0485	-0.0366		0.0407	0.230		
	(1.99)	(-8.4)	(-57.0)	(-4.6)	(-10.9)	(-58.3)			
		-4.136	-0.0529	0.0845					
		(4.68)	(8.18)	(12.7)					
Exact solution [24]	16.728	2.637	0.1135	-0.0350		0.0457	0.552		
		-3.951	-0.0489	0.0750					

<sup>a</sup> Percentage difference.

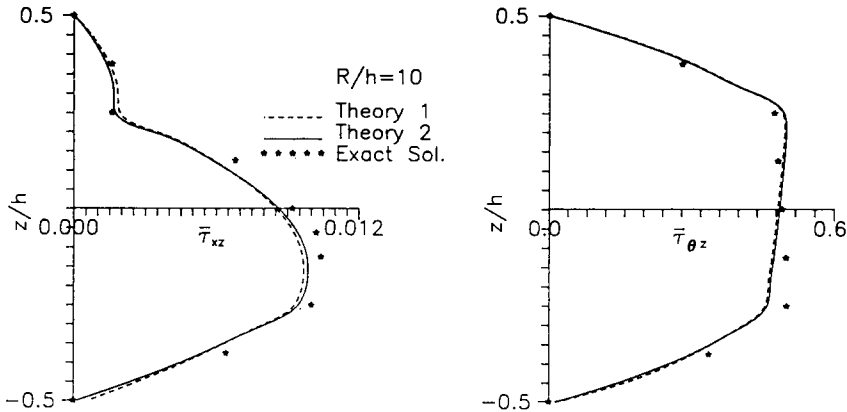


Fig. 4. Variation of transverse shear stresses through the thickness for a  $0^\circ/90^\circ/0^\circ$  shell with  $R/h = 10$ .

sional solutions, in general. Further, the estimates of the transverse shear stresses are better obtained with the central difference (CD) algorithm.

*Example 2*

A pressurized two-layer, circular cylindrical shell, which is supported at both ends in such a way that only the radial deflection and the circumferential rotation are restrained, is analyzed. The length and the inner radius of the shell are 20 in. and 10 in., respectively. The inner layer has a fibre orientation in the longitudinal direction  $90^\circ$  while the fibre orientation in the outer layer is varied. The layers are of equal thickness and the elastic properties of the lamina are given as follows:

$$E_1 = 40 \times 10^6 \text{ psi}, \quad E_2 = E_3 = 10^6 \text{ psi}, \quad \nu_{12} = \nu_{23} = \nu_{13} = 0.25,$$

$$G_{12} = G_{23} = G_{13} = 0.5 \times 10^6 \text{ psi}.$$

The thickness of shell  $h$  is taken as 0.2 in. and the fibre orientations of the outer layer are kept at  $-75^\circ$  and  $90^\circ$ . The variation of transverse shear stress ( $\bar{\tau}_{xz} = \tau_{xz}/p$ ) across the thickness, near the support is plotted in Fig. 6. The values given by Chaudhuri [25] are also shown for comparison.

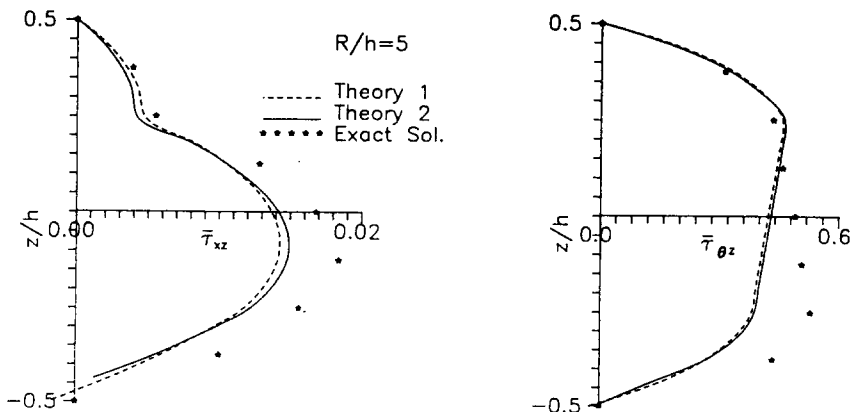


Fig. 5. Variation of transverse shear stresses through the thickness for a  $0^\circ/90^\circ/0^\circ$  shell with  $R/h = 5$ .

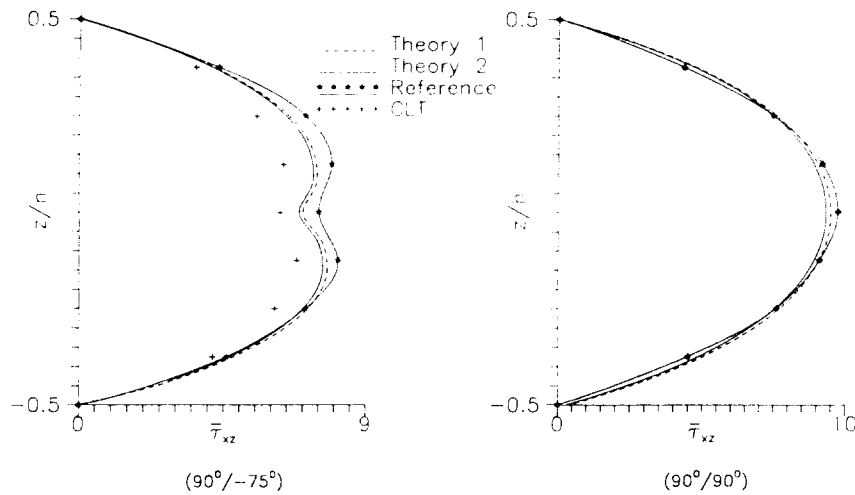


Fig. 6. Variation of transverse shear stresses through the thickness of a pressurized two-layer shell.

In the present analysis, half of the shell is discretized into 44 elements (four elements along the circumference and eleven elements along the length) in the case of non-axisymmetric behaviour. Only 1/16th of the shell is taken in the case of cross-ply laminates exhibiting axisymmetric behaviour and these are discretized with only 20 elements. As against this, Chaudhuri [25] has used 144 triangular elements in his analysis which uses another high-order theory. Our results are in close agreement with those of Chaudhuri.

Table 4

Maximum displacements ( $\bar{u}_3$ ) and normal stress ( $\bar{\sigma}_\theta$ ) for a simply supported three-layered sandwich cylindrical shell panel under sinusoidal transverse load for difference  $R/h$  ratios

$R/h$	$\bar{u}_3$					$\bar{\sigma}_\theta (\pm h/2)$				
	FOST		Present		3-D exact [26]	FOST		Present		3-D exact [26]
	Theory 1	Theory 2	Theory 1	Theory 2		Theory 1	Theory 2	Theory 1	Theory 2	
100	1.561 (-29.3) <sup>a</sup>	1.554 (-29.7)	2.085 (-4.3)	2.075 (-6.1)	2.211	1.048 (-9.3)	1.042 (-9.8)	1.153 (-0.3)	1.146 (-0.8)	1.156
						-1.050 (-9.2)	-1.046 (-9.6)	-1.152 (-0.4)	-1.148 (-0.8)	-1.157
10	1.646 (-28.8)	1.567 (-32.2)	2.097 (-9.3)	1.994 (-13.7)	2.312	0.991 (-8.5)	0.939 (-13.3)	1.053 (-2.7)	0.994 (-8.2)	1.083
						-0.997 (-7.9)	-0.964 (-10.9)	-1.032 (-4.7)	-1.002 (-7.4)	-1.083
5	1.738 (-20.5)	1.570 (-28.2)	1.937 (-11.4)	1.744 (-20.2)	2.186	0.718 (0.0)	0.652 (-9.2)	0.682 (-3.0)	0.616 (-14.2)	0.718
						-0.669 (10.6)	-0.632 (4.46)	-0.592 (-2.1)	-0.568 (-6.1)	-0.605
2	0.321 (-28.5)	0.227 (-49.5)	0.354 (-21.1)	0.251 (-44.0)	0.449	-0.213 (52.1)	-0.146 (4.3)	-0.201 (43.5)	-0.132 (-5.7)	-0.140
						0.425 (-14.1)	0.338 (-31.7)	0.398 (-19.6)	0.323 (-36.7)	0.495

<sup>a</sup> Percentage difference.

Table 5  
Maximum shear stress ( $\bar{\tau}_{\theta z}$  and  $\bar{\tau}_{xz}$ ) for a simply supported three-layered sandwich cylindrical shell panel under sinusoidal transverse load for different  $R/h$  ratios at ( $z = 0$ )

S	Models	$\tau_{\theta z}$				$\tau_{xz}$				
		Theory 1		Theory 2		Theory 1		Theory 2		
		FD	CD	FD	CD	FD	CD	FC	CD	
100	FOST	0.319 (5.9) <sup>a</sup>	0.303 (0.6)	0.316 (4.9)	0.300 (-0.3)	0.0415 (-21.5)	0.0394 (-25.5)	0.0411 (-22.3)	0.0391 (-26.0)	
	Present	0.311 (3.2)	0.293 (-2.6)	0.308 (2.3)	0.290 (-3.6)	0.0511 (-0.3)	0.0485 (-8.3)	0.0506 (-4.3)	0.0480 (-9.3)	
	3-D Exact [26]	0.301				0.0529				
	10	FOST	0.294 (4.2)	0.278 (-1.4)	0.267 (-5.3)	0.253 (-10.3)	0.0405 (-25.2)	0.0384 (-29.2)	0.0373 (-31.2)	0.0355 (-34.5)
10	Present	0.283 (0.3)	0.266 (-5.6)	0.256 (-9.2)	0.241 (-14.5)	0.0477 (-11.9)	0.0453 (-16.4)	0.0440 (-18.2)	0.0418 (-22.8)	
	3-D Exact [26]	0.282				0.0542				
	5	FOST	0.217 (24.7)	0.206 (18.3)	0.177 (1.73)	0.167 (-4.0)	0.0373 (-21.9)	0.0355 (-25.7)	0.0326 (-31.8)	0.0310 (-35.1)
	5	Present	0.193 (10.9)	0.181 (4.0)	0.156 (10.3)	0.146 (16.0)	0.0392 (-17.9)	0.0372 (-22.1)	0.0342 (-28.4)	0.0325 (-32.0)
3-D Exact [26]		0.174				0.0478				
2		FOST	0.030 (61.3)	0.029 (55.9)	0.024 (29.0)	0.022 (18.2)	0.0026 (-36.5)	0.0025 (-39.0)	0.0027 (-34.1)	0.0026 (-36.6)
2		Present	0.021 (12.9)	0.019 (2.1)	0.017 (-8.6)	0.016 (-13.9)	0.0040 (-2.4)	0.0033 (-19.5)	0.0033 (-19.5)	0.0032 (-21.9)
	3-D Exact [26]	0.0186				0.0041				

<sup>a</sup> Percentage difference.

Example 3

An analysis of a three-layered sandwich circular cylindrical shell panel with simple supports at all the four edges is carried out and the results obtained are compared with a three-dimensional elasticity solution obtained by Kant and Reddy [26]. The shell roof has an arc length  $a = 10$  in., a length  $L = 10$  in. and a thickness  $h = 1.0$  in (see Fig. 3). A sinusoidal load,  $p = p_0 \sin(\pi R\theta/a) \sin(\pi x/L)$  is applied on the top shell surface. The material property coefficients for the facings are,

$$E_1 = 25E_2, \quad E_2 = E_3; \quad G_{12} = G_{13} = 0.5E_2, \quad G_{23} = 0.2E_2, \quad \nu_{12} = \nu_{13} = \nu_{23} = 0.25, \\ \text{facing thickness } t_f = 0.1h.$$

The properties of the core are taken as follows:

$$E_1 = E_2 = 0.04 \times 10^6 \text{ psi}, \quad E_3 = 0.5 \times 10^6 \text{ psi}, \\ G_{13} = G_{23} = 0.6 \times 10^6 \text{ psi}, \quad G_{12} = 0.016 \times 10^6 \text{ psi}, \\ \nu_{12} = 0.25, \quad \nu_{23} = \nu_{13} = 0.02 \\ \text{core thickness } t_c = 0.8h.$$

Numerical results are obtained for different  $R/h$  ratios, namely 100, 10, 5 and 2. Normalized maximum deflection and stresses are given in Tables 4 and 5. The percentage difference between the present and the elasticity solutions is also given in these tables. The maximum

deflection and normal stresses at the center and transverse shear stresses at supports are normalized as follows:

$$\bar{\sigma}_\theta = \frac{h^2}{\rho_0 a^2} \sigma_\theta, \quad (\bar{\tau}_{\theta z}, \bar{\tau}_{xz}) = (\tau_{\theta z}, \tau_{xz}) h / \rho_0 a,$$

$$\bar{u}_3 = \frac{E_2 h^3}{\rho_0 a^4} 100 u_3.$$

The results are seen to be very close to the three-dimensional solutions even for low values of the  $R/h$  ratio.

## Conclusions

The results from two higher-order theories of a laminated composite cylindrical shell subjected to different loadings and boundary conditions are presented. The displacement model contains the minimum number of displacement parameters so as to incorporate non-linear variation of displacements, stresses and strains through the thickness. These theories do not require the use of a shear correction factor. The finite element method is employed for global analysis involving evaluation of the displacements and in-plane stresses. In the post-processing phase, two special finite-difference-based algorithms are developed and presented here for the first time. These are implemented in the general software for the direct integration of the three-dimensional stress equilibrium equations. This methodology has led to a reliable evaluation of transverse/interlaminar stresses in a routine manner.

The results obtained show excellent agreement with the elasticity solutions. It is also observed that the Theory 2 provides more reliable and accurate results compared to Theory 1 and is generally closer to an elasticity solution for thick shells. Thus the influence of  $h/R$  ratio in the strain–displacement relations is established especially for thick shells.

## References

- [1] W. FLÜGGE, *Stresses in Shells*, Springer-Verlag, New York, 4th edn., 1967.
- [2] H. KRAUS, *Thin Elastic Shells*, Wiley, New York, 1967.
- [3] P.M. NAGHDI, "A survey of recent progress in the theory of elastic shells", *Appl. Mech. Rev.* **9**, pp. 365–368, 1956.
- [4] S.B. DONG, K.S. PISTER and R.L. TAYLOR, "On the theory of laminated anisotropic shells and plates", *J. Aerosp. Sci.* **29**, pp. 969–975, 1962.
- [5] R.A. CHAUDHURI, K. BALARAMAN and V. KUNUKKASSERIAL, "Arbitrary laminated anisotropic cylindrical shells under internal pressure", *AIAA J.* **24**, pp. 1851–1857, 1986.
- [6] R.C. REUTER, "Analysis of shells under internal pressure", *J. Compos. Mater.* **6**, pp. 94–113, 1972.
- [7] S.B. DONG and F.K.W. TSO, "On a laminated orthotropic shell theory including transverse shear deformation", *ASME J. Appl. Mech.* **39**, pp. 1091–1097, 1972.
- [8] S.C. PANDA and R. NATARAJAN, "Finite element analysis of laminated shells of revolution", *Comput. Struct.* **6**, pp. 61–64, 1976.
- [9] J.N. REDDY, "Exact solution of moderately thick laminated shells", *ASCE J. Eng. Mech. Div.* **108**, pp. 794–809, 1984.
- [10] Abu-Arja KAMAL, Static analysis of laminated fiber reinforced plates and shells with shear deformation. Ph.D. Thesis, Department of Civil Engineering University of Utah, 1987.
- [11] P. SEIDE and R.A. CHAUDHURI, "Triangular finite element for analysis of thick laminated shells", *Int. J. Numer. Methods Eng.* **24**, pp. 1563–1579, 1987.
- [12] J.M. WHITNEY and C.T. SUN, "A higher-order theory for extensional motion of laminated anisotropic plates and shells", *J. Sound Vib.* **30**, pp. 85–88, 1971.

- [13] J.M. WHITNEY and C.T. SUN, "A refined theory for laminated anisotropic cylindrical shells", *ASME J. Appl. Mech.* **41**, pp. 471–476, 1974.
- [14] T. KANT, Thick shells of revolution—Some studies, Ph.D. Thesis, Department of Civil Engineering Indian Institute of Technology Bombay, India, 1976.
- [15] A. BHIMARADDI, "A higher order theory for free vibration analysis of circular cylindrical shells", *Int. J. Solids Struct.* **20**, pp. 623–630, 1984.
- [16] A. BHIMARADDI and L.K. STEVENS, "On the higher-order theories in plates and shells", *Int. J. Struct.* **6**, pp. 35–50, 1986.
- [17] A.V.K. MURTY and T.S.R. REDDY, "A higher-order theory for laminated composite cylindrical shells", *J. Aeronaut. Soc. India*, pp. 161–171, 1986.
- [18] T. KANT and M.P. MENON, "Higher-order theories for composite and sandwich cylindrical shell with  $C^0$  finite elements", *Comput. Struct.* **33**, pp. 1191–1204, 1989.
- [19] L.R. CALCOTE, *The Analysis of Laminated Composite Structures*, Von Nostrand Reinhold, New York, 1969.
- [20] B.N. PANDYA and T. KANT, "A refined higher-order generally orthotropic  $C^0$  plate bending element", *Comput. Struct.* **28**, pp. 119–133, 1988.
- [21] O.C. ZIENKIEWICZ and R.L. TAYLOR, *The Finite Element Method, Vol. 1: Basic Formulations and Linear Problems*, McGraw-Hill, London, 1989.
- [22] T. KANT, D.R.J. OWEN and O.C. ZIENKIEWICZ, "A refined higher order  $C^0$  plate bending element", *Comput. Struct.* **15**, pp. 177–183, 1982.
- [23] M.G. SALVADORI and M.L. BARON, *Numerical Methods in Engineering*, Prentice-Hall, Englewood Cliffs, NJ, 1961.
- [24] J.G. REN, "Analysis of simply supported laminated circular cylindrical shells", *Compos. Struct.* **11**, pp. 277–292, 1989.
- [25] R.A. CHAUDHURI, "On the prediction of interlaminar shear stresses in a thick laminated general shell", *Int. J. Solids Struct.* **26**, pp. 1499–1510, 1990.
- [26] T. KANT and T.S. REDDY, "Three dimensional elastostatic analysis of fibre reinforced composite laminated shells", Res. Rep. IITB/CE/R/92/2, Department of Civil Engineering, Indian Institute of Technology, Bombay, 1992.